RadioGraphics

Imaging Characteristics of Primary Osteosarcoma: Nonconventional Subtypes[1]

Gail Yarmish, MD • Michael J. Klein, MD • Jonathan Landa, DO
Robert A. Lefkowitz, MD • Sinchun Hwang, MD

CME FEATURE

See www.rsna.org/education/rg_cme.html

LEARNING OBJECTIVES FOR TEST 5

After reading this article and taking the test, the reader will be able to:

- List the imaging features of the less common nonconventional subtypes of primary osteosarcoma.
- Describe the differences in prognosis between the various subtypes of primary osteosarcoma.
- Discuss the imaging features that are useful in distinguishing between the nonconventional subtypes of primary osteosarcoma and other lesions, both benign and malignant.

TEACHING POINTS

See last page

Osteosarcoma (OS) is a common primary malignant tumor of bone that produces osteoid matrix. According to the World Health Organization, OS of bone is classified into eight subtypes with distinct biologic behaviors and clinical outcomes: conventional, telangiectatic, small cell, low-grade central, secondary, parosteal, periosteal, and high-grade surface. Imaging plays a crucial role in the diagnosis of each subtype of OS and ultimately in patients' survival because the diagnosis is based on a combination of histopathologic and imaging features. Conventional OS is the most common subtype of OS and is readily identified at radiography as an intramedullary mass with immature cloudlike bone formation in the metaphyses of long bones. The imaging features of less common subtypes of primary OS are variable and frequently overlap with those of multiple benign and malignant entities, creating substantial diagnostic challenges. For accurate diagnosis, it is important to be aware of radiographic and cross-sectional imaging features that allow differentiation of each nonconventional subtype of OS from its mimics.

Abbreviations: ABC = aneurysmal bone cyst, GCT = giant cell tumor, H-E = hematoxylin-eosin, OS = osteosarcoma

RadioGraphics 2010; 30:1653–1672 • **Published online** 10.1148/rg.306105524 • **Content Codes:** MK OI

[1]From the Department of Radiology, Memorial Sloan-Kettering Cancer Center, 1275 York Ave, New York, NY 10065 (G.Y., J.L., R.A.L., S.H.); Department of Radiology, Staten Island University Hospital, Staten Island, NY (G.Y.); and Department of Pathology and Laboratory Medicine, Hospital for Special Surgery, New York, NY (M.J.K.). Recipient of a Cum Laude award for an education exhibit at the 2009 RSNA Annual Meeting. Received April 23, 2010; revision requested May 24 and received June 30; accepted July 2. For this CME activity, the authors, editors, and reviewers have no relevant relationships to disclose. **Address correspondence to** G.Y. (e-mail: *gyarmish@gmail.com*).

Introduction

Osteosarcoma (OS) is a malignant tumor of connective tissue that produces osteoid matrix and variable amounts of cartilage matrix and fibrous tissue (1). Although it accounts for less than 1% of all cancers diagnosed in the United States, OS is the most common primary bone tumor in children and adolescents (4.4 cases per million persons per year) (2–4). The current World Health Organization classification of OS of bone includes eight categories: conventional, telangiectatic, small cell, low-grade central, secondary, parosteal, periosteal, and high-grade surface (5). Although conventional OS and secondary OS are histologically indistinguishable, diagnoses of conventional OS and secondary OS are made on the basis of typical radiographic appearances (ie, a destructive mass with cloudlike radiopacity in long bones and a mass arising from a preexisting abnormality such as Paget disease, respectively).

However, less common types of OS, which we refer to as nonconventional subtypes of OS, exhibit distinct imaging appearances mimicking those of many different benign and malignant entities. Because the therapeutic options and prognoses for different types of OS differ from each other, correct diagnosis is essential and requires recognition of characteristic imaging features. In this article, we review the imaging characteristics and differential diagnostic considerations of the nonconventional subtypes of OS (parosteal, periosteal, high-grade surface, telangiectatic, small cell, low-grade central) and a variety of benign and malignant diagnostic entities that mimic them.

Juxtacortical Osteosarcoma

Juxtacortical or surface OS refers to OS originating from the surface of bone. It is primarily associated with the periosteum, with variable medullary canal involvement. The term *juxtacortical osteosarcoma* was initially used to describe parosteal OS. In 1992, after various types of surface OS that exhibited distinctive histopathologic features and biologic behaviors were recognized, the World Health Organization redefined the classification of "juxtacortical osteosarcoma" to include all surface types of OS (5). Juxtacortical OS is now classified into three main subtypes—parosteal, periosteal, and high-grade surface OS—and these are further categorized by their histologic features and histologic grade.

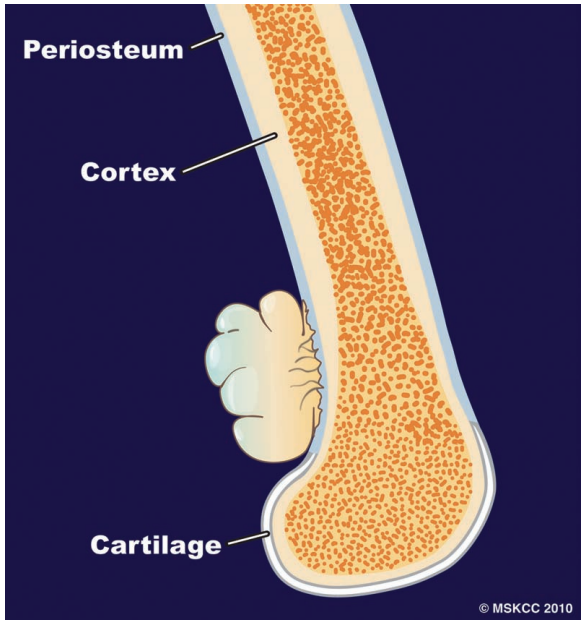

Figure 1. Drawing of parosteal OS shows that the tumor is typically lobular and arises from the outer periosteum of the metaphysis of a long bone.

Parosteal Osteosarcoma

Parosteal OS is the most common type of juxtacortical OS, accounting for approximately 5% of all OS cases and typically manifesting in the 2nd to 4th decades of life (2,6). The tumor usually occurs in the metaphyses of long bones (Fig 1), and the posterior aspect of the distal femur is the most frequent site (about 62% of cases) (7,8). The prognosis for parosteal OS is better than that for conventional OS, as the 5-year overall survival rate is 86%–91% for the former but 53%–61% for the latter (2,3,9).

Anatomically, parosteal OS originates from the outer fibrous layer of the periosteum (Fig 2) and is usually low grade, exhibiting minimal fibroblastic stromal atypia and extensive bone matrix (1). The bone matrix is often arranged in long parallel streamers reminiscent of a hair-on-end periosteal reaction outside of the periosteum.

At radiography, the classic appearance is a lobulated and exophytic mass with central dense ossification adjacent to the bone (Fig 3). A cleavage plane separating the tumor and adjacent

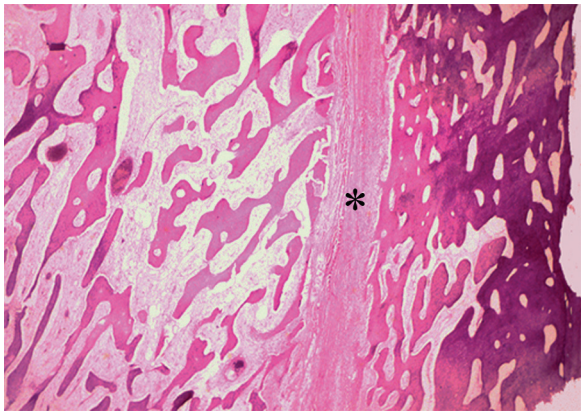

Figure 2. Histologic features of parosteal OS. Photomicrograph (original magnification, ×25; hematoxylin-eosin [H-E] stain) shows periosteum (*) interposed between the low-grade bone-producing tumor (to the left of the periosteum) and underlying bone (to the right of the periosteum). The tumor is usually low grade and consists of fibroblastic stroma with minimal atypia and extensive bone matrix, which is often arranged in trabecular streamers.

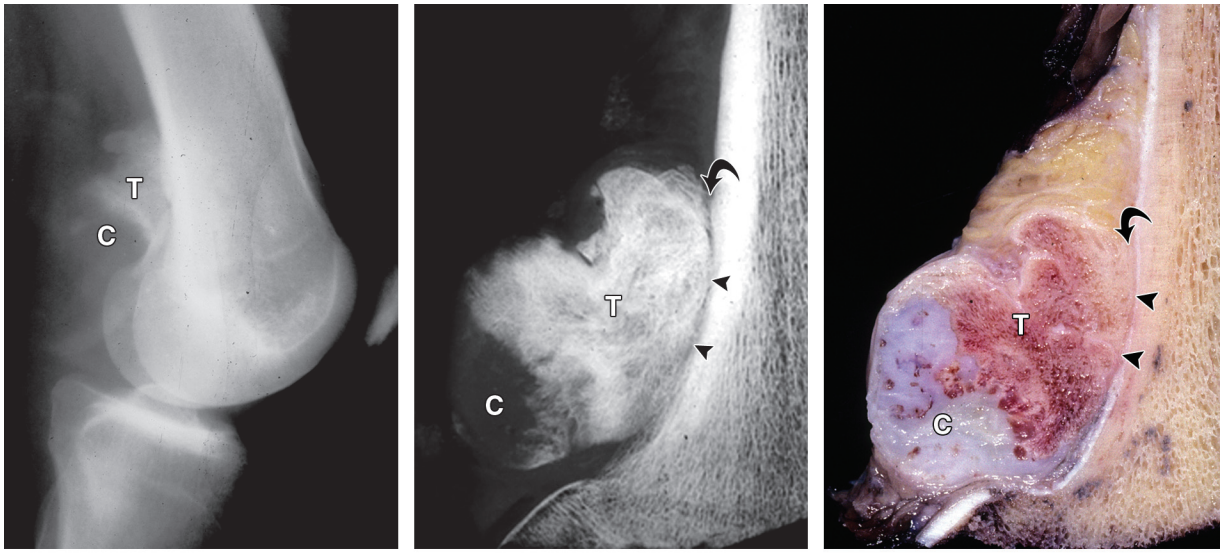

a. **b.** **c.**

Figure 3. Parosteal OS of the distal femur in a 29-year-old man. Radiograph of the knee **(a)** and radiograph **(b)** and photograph **(c)** of a sagittal section of the gross specimen show an ossified exophytic tumor *(T)* on the surface of the femur. A lucent cleavage plane (arrow in **b** and **c**) is seen at the edge of the tumor. The tumor is centrally ossified and contains chondroid tissue *(C)*. A thin lucent line (arrowheads in **b** and **c**) is seen between the tumor and underlying bone and corresponds to the periosteum (shown in Fig 2).

normal cortex (also known as the string sign) (Fig 3) has been reported in approximately 30% of cases at radiography (6) and in 65% of cases at cross-sectional imaging (7). This cleavage plane corresponds histologically to the periosteum interposed between the cortex and the tumor mass (Fig 2). Cortical thickening with a relative lack of aggressive periosteal reaction is often apparent, due to focal expansion of the inner portion of the tumor and fusion with the cortex.

At cross-sectional imaging, invasion into the medullary canal is frequently observed in both low-grade (41%) and high-grade (50%) lesions, and its effect on prognosis is controversial (7). At magnetic resonance (MR) imaging, the ossified tumor is predominantly low in signal intensity on both T1- and T2-weighted images, similar to the appearance of the cortex, owing to lack of mobile protons that produce MR signal (Fig 4). When there is an unmineralized soft-tissue mass larger than 1 cm^3 or the lesion is predominantly high in T2 signal intensity, the tumor is more likely to be of high grade (7).

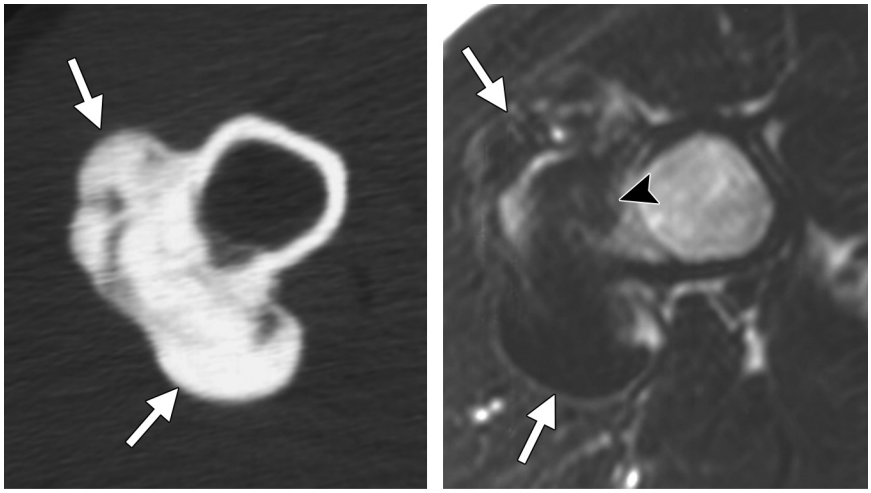

a. b.

Figure 4. Parosteal OS of the proximal humerus in a 28-year-old man. **(a)** Axial computed tomographic (CT) image of the humerus shows an exophytic and heavily ossified tumor (arrows) at the cortex. **(b)** Axial T2-weighted MR image shows predominantly low signal intensity in the ossified tumor (arrows), an appearance similar to that of the cortex. The signal intensity of the tumor was also low on axial T1-weighted MR images. There is a focal intramedullary extension (arrowhead), which was confirmed at histologic analysis.

Dedifferentiation of low-grade parosteal OS to high-grade disease has been reported in 16%–43% of cases (10–12). Histologically, these tumors consist of an admixture of low-grade parosteal OS and a second component that is either a higher-grade OS or a sarcoma of different histologic type. Dedifferentiation has been observed with equal frequency at initial diagnosis and at local recurrence (10,11). Among the histologic types of dedifferentiated parosteal OS, high-grade conventional OS is the most common followed by fibrosarcoma and malignant fibrous histiocytoma (1,6). Dedifferentiation correlates radiographically with increased lysis and the presence of a soft-tissue mass without ossification (Fig 5) (7,11,12).

Differential diagnostic considerations for parosteal OS include benign entities such as osteochondroma, myositis ossificans, and periosteal chondroma and malignant entities such as fibrous malignancy, periosteal chondrosarcoma, and other subtypes of juxtacortical OS (discussed in more detail later in the article). Osteochondroma and myositis ossificans are common mimics of parosteal OS. Osteochondroma is considered the most common benign tumor of bone, constituting 20%–50% of all benign bone tumors, and may be developmental or associated with trauma or irradiation (13). The diagnostic imaging feature of osteochondroma is corticomedullary continuity of a juxtacortical bone lesion with the adjacent bone, with or without a hyaline cartilage cap.

MR imaging is the best imaging modality for evaluating osteochondroma (Fig 6). The cartilage cap demonstrates high signal intensity at T2-weighted or proton-density imaging owing to its high water content. In contrast to osteochondroma, parosteal OS lacks corticomedullary continuity between the tumor and the underlying medullary canal (Fig 7). Although parosteal OS occasionally demonstrates cartilage tissue with a caplike appearance on MR images, it is often irregular, incomplete, and thick (Fig 7) (14), in contrast to the smooth, continuous, and relatively thin cartilage cap of an osteochondroma.

Teaching Point

At histologic analysis, the cartilage cap of an osteochondroma resembles the histologic appearance of the growth plate; the underlying bone contains normal marrow fat and is formed by endochondral ossification. Conversely, in parosteal OS, the cartilage tissue is often more cellular and the underlying bone contains fibrous tissue between the trabeculae rather than marrow.

Myositis ossificans is a benign ossified soft-tissue mass within muscle that can be atraumatic or traumatic in origin. Gradual ossification of the lesion from the periphery toward the center of the mass is a characteristic radiographic finding of myositis ossificans (Fig 8). At histologic analysis, this progressive maturation from central

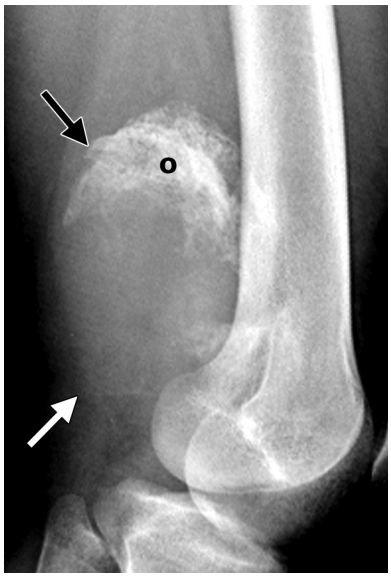

Figure 5. Dedifferentiated parosteal OS in a 16-year-old girl. Radiograph shows a tumor (arrows) in the posterior distal femur. The tumor is predominantly soft tissue with only a small area of ossification *(O)* owing to lack of bone production in the chondroblastic dedifferentiation.

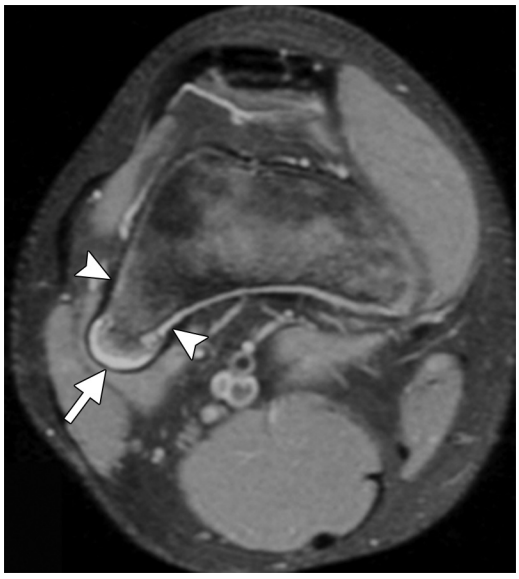

Figure 6. Osteochondroma in a 14-year-old boy. Axial fat-suppressed proton-density–weighted MR image shows a smooth cartilaginous cap of high signal intensity (arrow) in the distal femur. There is corticomedullary continuity (arrowheads) with the adjacent femur.

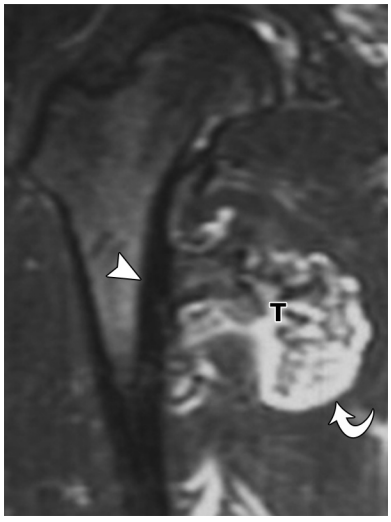

Figure 7. Parosteal OS mimicking osteochondroma in a 25-year-old man. Coronal fat-suppressed T2-weighted MR image shows a tumor *(T)* in the proximal femur. The tumor has a long stalk, a feature that mimics the appearance of an osteochondroma. However, there is a thickened cortex (arrowhead) that separates the tumor from the medullary canal of the femur. The cartilaginous cap (arrow) is irregular and thickened.

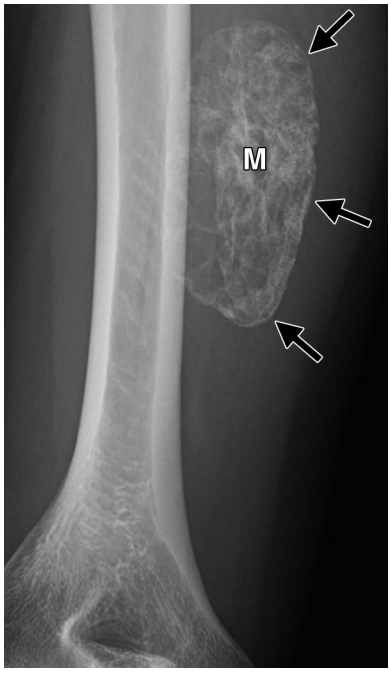

Figure 8. Myositis ossificans in a 23-year-old woman. Radiograph of the humerus shows a well-circumscribed soft-tissue mass *(M)* with peripheral calcifications (arrows), an appearance known as the zoning phenomenon. Initial radiography did not reveal the mass. The patient experienced trauma in this area 2 months earlier.

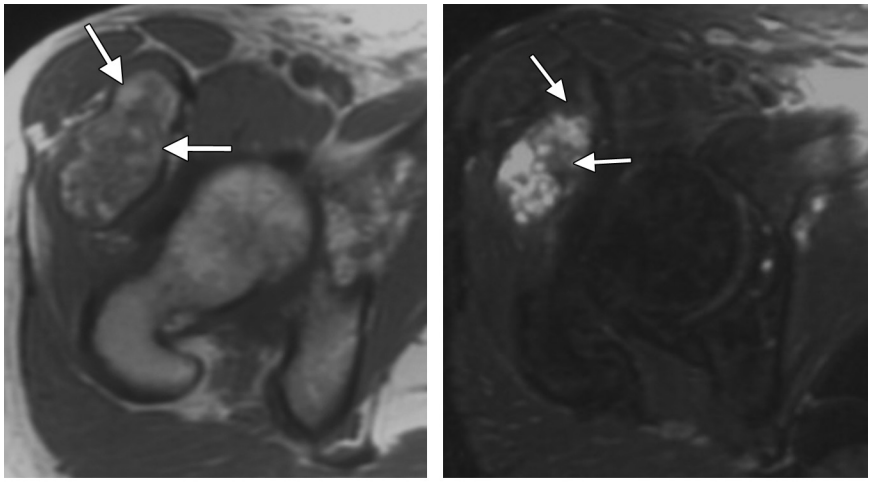

a. b.

Figure 9. Myositis ossificans in a 34-year-old woman. Axial T1-weighted **(a)** and axial T2-weighted fat-suppressed **(b)** MR images of the thigh show a soft-tissue mass that contains areas of high T1 and low T2 signal intensity (arrows), findings consistent with fat. The remainder of the mass, with heterogeneous T1 and T2 signal intensity and without a signal drop on the fat-suppressed image, represents evolving hemorrhage. The mass developed after a fall a few months earlier.

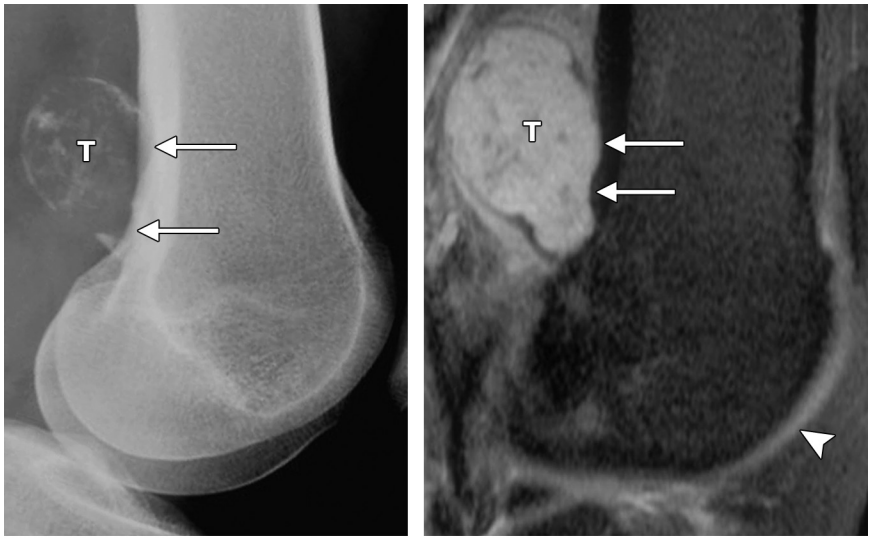

a. b.

Figure 10. Periosteal chondroma in a 36-year-old woman. Radiograph **(a)** and sagittal T2-weighted MR image **(b)** show a juxtacortical mass *(T)* with cortical saucerization (arrows) in the distal femur. The lucent radiographic appearance with peripheral curvilinear calcifications and the high T2 signal intensity similar to that of cartilage (arrowhead in **b**) are consistent with a chondroid neoplasm.

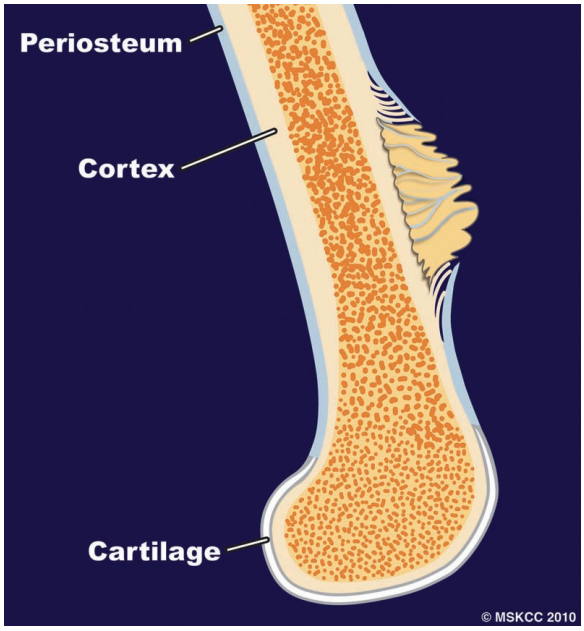

Figure 11. Drawing of periosteal OS shows that the tumor most commonly arises from the inner periosteum of the diaphysis of a long bone and demonstrates perpendicular periosteal reaction.

cellular osteoid foci to peripheral lamellar mature bone is known as the zoning phenomenon (15). The ossification pattern of parosteal OS is the radiographic inverse of that seen in myositis ossificans, with the densest ossification in the center of the lesion and the least radiopaque bone at the periphery (Fig 3).

Teaching Point

At MR imaging, myositis ossificans may simulate malignancy in the early to intermediate phases (2–8 weeks), appearing as an enhancing soft-tissue mass with surrounding edema; the emergence of mature ossification in the late phase is diagnostic of myositis ossificans (Fig 9) (15). The presence of prominent surrounding edema is also a differentiating feature from parosteal OS.

Periosteal chondroma and periosteal chondrosarcoma are rare juxtacortical chondroid tumors that arise in the deep layer of the periosteum. Periosteal chondroma typically occurs on the metaphyseal surfaces of long bones (16,17). At radiography, periosteal chondroma is a radiolucent lesion with variable degrees of chondroid matrix calcifications (Fig 10). Owing to its origins in the deep layer of the periosteum, periosteal chondroma typically causes cortical saucerization (Fig 10) with a well-formed periosteal reaction, findings unusual in parosteal OS.

At MR imaging, periosteal chondroma is a rounded mass with hyperintense T2 signal due to high water content in the chondroid matrix; adjacent marrow edema is uncommon (Fig 10) (16,17). Distinguishing periosteal chondroma from periosteal chondrosarcoma at imaging is challenging because the aforementioned imaging features overlap and intramedullary extension and edema are rare in both entities, although they are slightly more frequent in periosteal chondrosarcoma (16,17). In a few small studies, the most reliable predictor of periosteal chondrosarcoma was its size, which was usually greater than 4 cm (16,17).

Periosteal Osteosarcoma

Periosteal OS is the second most common type of juxtacortical OS, accounting for 1.5% of all OS cases (2). It typically affects patients in the 2nd or 3rd decade of life, with a characteristic location along the diaphyses of long bones (Fig 11), most commonly the tibia (18). The prognosis for periosteal OS (83% 5-year survival rate) is better than that for conventional OS but worse than that for parosteal OS (19).

Periosteal OS arises from the inner, germinative layer of periosteum (Fig 12). The tumor is predominantly cartilaginous, and its cytologic grade is intermediate, or grade 2 (1)—a grade distinctly lower than that of conventional OS but higher than that of parosteal OS. Common radiographic findings include a soft-tissue mass with periosteal reaction, cortical erosion, and cortical thickening (Fig 13). Although intramedullary extension of periosteal OS is a well-recognized entity, with

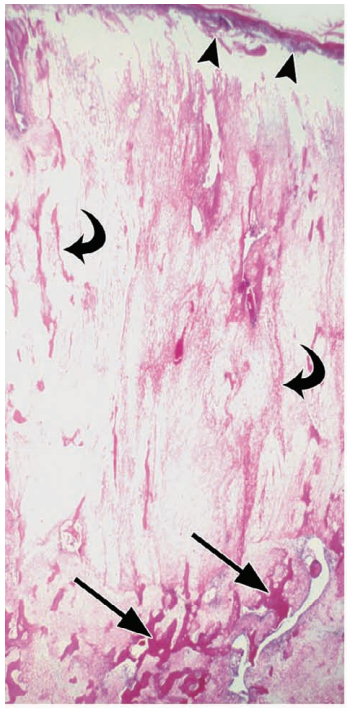

12.

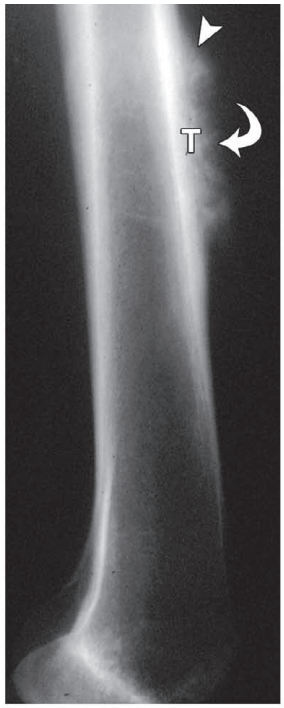

13a.

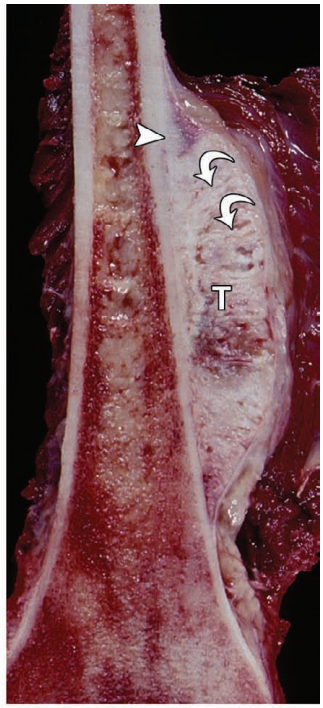

13b.

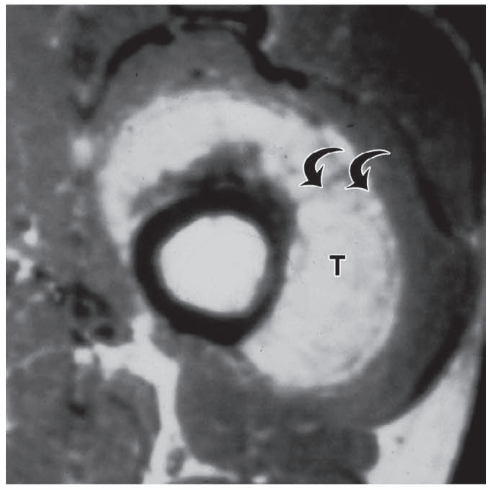

13c.

Figures 12, 13. **(12)** Histologic features of periosteal OS. Photomicrograph (original magnification, ×25; H-E stain) shows characteristic perpendicular streamers of bone matrix (curved arrows) and foci of neoplastic cartilage between the outer periosteum (arrowheads) and the deep portion of the tumor, in which there is bone matrix (straight arrows). **(13)** Periosteal OS in a 19-year-old man. Lateral radiograph **(a)**, photograph of a coronal section of the gross specimen **(b)**, and axial T2-weighted MR image **(c)** show a tumor *(T)* in the femoral diaphysis with a Codman triangle (arrowhead in **a** and **b**) at its edge and perpendicular periosteal reaction (arrows). (Fig 13a and 13c reprinted, with permission, from reference 1.)

several reports in the literature (18,19), it is still considered rare. Periosteal reaction often extends perpendicularly from the inner cortex to the outer margin of the tumor (Fig 13). The predominantly chondroid matrix of this tumor results in a lesion that is low in attenuation on CT images and hyperintense on T2-weighted MR images (Fig 13), with smaller foci of low signal intensity on MR images representing calcified matrix or hair-on-end periosteal reaction.

Considerations in the radiologic diagnosis of periosteal OS include other types of juxtacortical OS and periosteal chondroid tumors. Parosteal

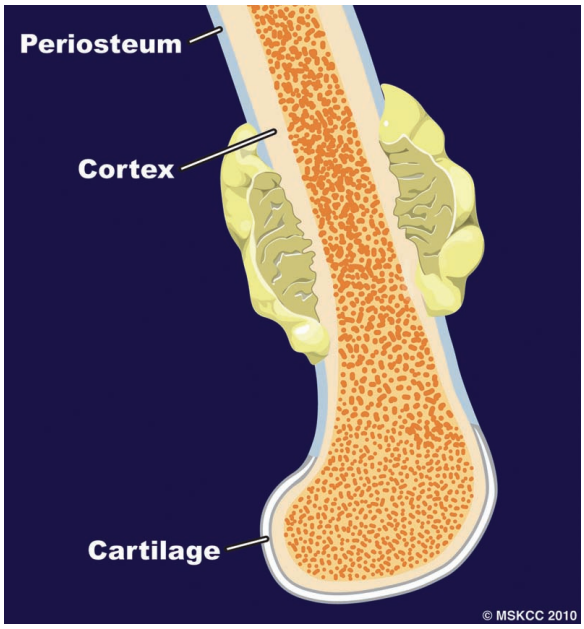

Figure 14. Drawing of high-grade surface OS shows that the tumor usually arises from the surface of the metaphysis or diaphysis of a long bone and may encase the bone circumferentially.

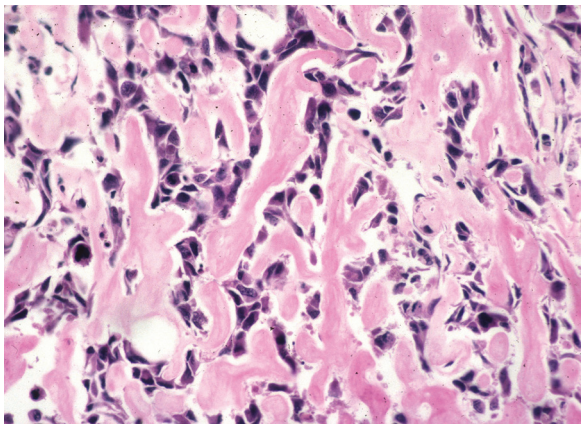

Figure 15. Histologic features of high-grade surface OS. Photomicrograph (original magnification, ×157; H-E stain) shows bulky streamers of bone produced by highly atypical polyhedral and spindle-shaped tumor cells.

OS is a densely ossified juxtacortical mass that lies outside the cortex and occurs in metaphyses (Figs 3, 4), whereas periosteal OS is usually more lytic in appearance, causing cortical erosion and periosteal reaction, and occurs in diaphyses (Fig 13).

Differentiation of high-grade surface OS from periosteal OS may be difficult at imaging, as both can occur in diaphyses and cause periosteal reaction and bone destruction. However, high-grade surface OS often involves the entire circumference of the cortex and is more likely to show medullary invasion (18). Furthermore, the presence of a high histologic grade, identical to that of conventional OS, throughout the entire tumor is diagnostic of high-grade surface OS.

Teaching Point

Periosteal chondroid tumors are juxtacortical soft-tissue masses with well-defined borders, typically metaphyseal in location, and contain curvilinear calcifications along the periphery of the cartilage lobules (17) (Fig 10); in contrast, periosteal OS is a broad-based soft-tissue mass, commonly diaphyseal in location, and produces a cortical erosion and periosteal reaction perpendicular to the cortex (18).

High-Grade Surface Osteosarcoma

High-grade surface OS is rare, accounting for 0.4% of all OS cases (2), and is the least common type of juxtacortical OS. The tumor affects patients in the 2nd and 3rd decades of life (20). Common locations include the diaphyses and metaphyses of long bones (Fig 14), with the femur being the most common site (20–22). The tumor is usually large, ranging from 4.5 to 22 cm (20–22). The prognosis for high-grade surface OS was initially considered worse than that for other types of juxtacortical OS and similar to that for conventional OS (21), with a reported 5-year survival rate of 46.1%; however, more recent studies have shown an improved prognosis that is better than that for conventional OS, probably due to aggressive chemotherapy and surgical resection (20,22).

At pathologic analysis, high-grade surface OS arises from the surface of bone; however, unlike the other forms of juxtacorcal OS, it is entirely high grade, with a high mitotic activity identical to that of conventional OS (Fig 15). At radiography, dense ossification and periosteal reaction are seen in the majority of cases (20,22); cortical

erosion and thickening are also seen frequently (Fig 16). The rate of intramedullary invasion is variable among small studies, occurring in anywhere from 8% to 48% of cases (20–22), but its presence has not been found to decrease the survival rate (21,22).

Imaging mimics of high-grade surface OS include parosteal OS, periosteal OS, and conventional OS. High-grade surface OS may resemble either parosteal OS with ill-defined and fluffy bone formation or periosteal OS when it is diaphyseal and associated with cortical destruction and periosteal reaction, depending on degrees of osteoblastic and chondroblastic differentiation (18,20,22). Circumferential bone involvement can be more extensive in high-grade surface OS (18) than in other forms of juxtacortical OS. When medullary invasion is a prominent feature, it may be difficult to distinguish this tumor from conventional OS with a large extraosseous component. However, to make the diagnosis of high-grade surface OS, the bulk of the lesion must be external to the bone at radiography.

Telangiectatic Osteosarcoma

Telangiectatic OS accounts for 1.2%–7.0% of all OS cases and most commonly occurs in the 1st and 2nd decades of life (3,23). The tumor occurs most often in metaphyses of long bones, with the femur being the most common site (23,24) (Fig 17). Since the introduction of neoadjuvant chemotherapy in 1975, the prognosis for telangiectatic OS has substantially improved. The 5-year survival rate has increased from 17% to 67%, approaching that of conventional OS (1,23,25). The favorable response for telangiectatic OS to chemotherapy may be related to the increased growth fraction of tumor cells compared with that in conventional OS, since most chemotherapeutic agents used for OS are cell cycle specific (26).

At pathologic analysis, hemorrhagic, cystic, or necrotic spaces occupy more than 90% of the tumor, with only a small fraction of solid tissue (Fig 18) (1). Therefore, at low power, telangiectatic OS mimics aneurysmal bone cyst (ABC). Bone matrix is scant, accounting for the characteristic radiolucent appearance of the tumor. At high magnification, the presence of cells with significant nuclear pleomorphism and a high mitotic rate as well as the presence of osteoid matrix, albeit scarce, enable one to make a specific histologic diagnosis (1).

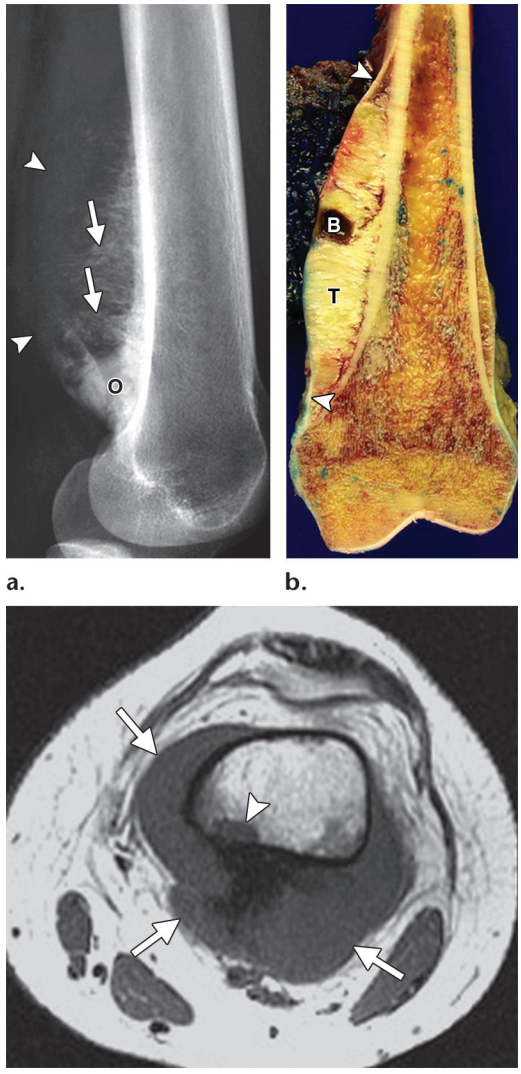

Figure 16. High-grade surface OS in a 19-year-old woman. **(a)** Radiograph shows ossification *(O)* and periosteal reaction (arrows) within a tumor (arrowheads) along the surface of the distal femur. **(b)** Photograph of a coronal section of the gross specimen shows lifting of the periosteum (arrowheads) by the tumor *(T)*. *B* = biopsy defect. **(c)** Axial T1-weighted MR image shows that the tumor (arrows) surrounds the femur circumferentially and invades the medullary canal focally (arrowhead). Histologic analysis showed a diffusely high-grade neoplasm with intramedullary extension.

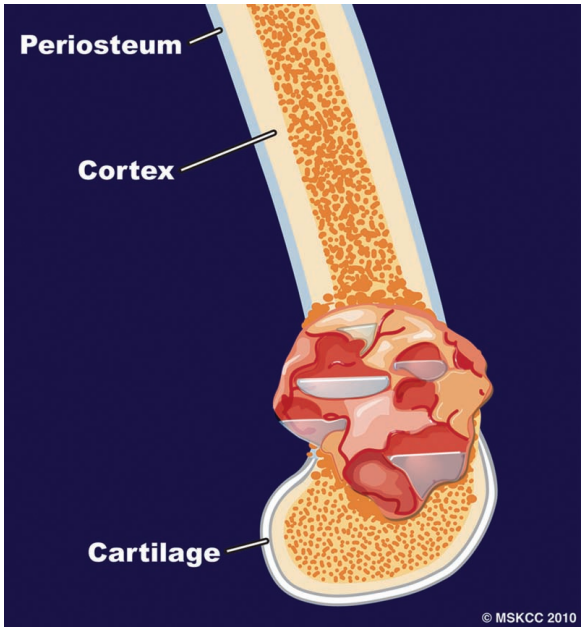

Figure 17. Drawing of telangiectatic OS shows that the tumor usually arises from the metaphysis of a long bone and is expansile and lytic. It contains multiple fluid levels due to layering hemorrhage.

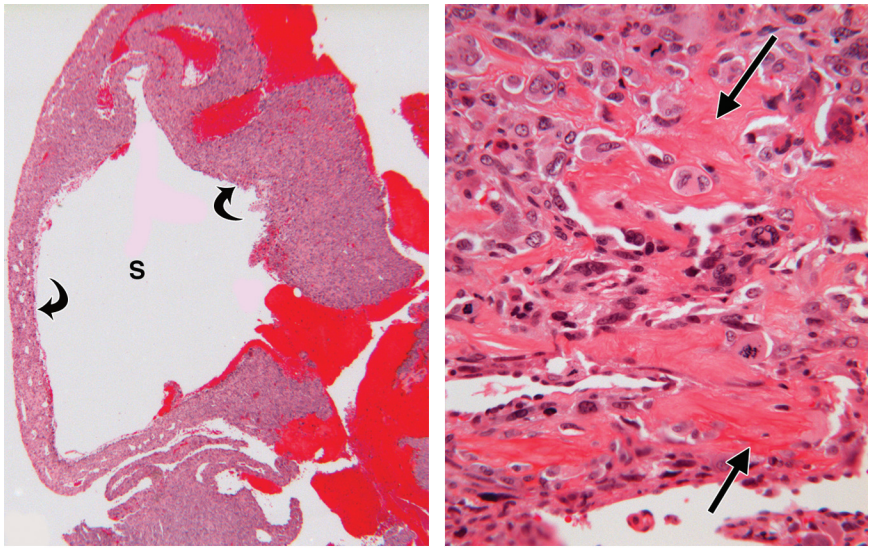

a. **b.**

Figure 18. Histologic features of telangiectatic OS. **(a)** Low-power photomicrograph (original magnification, ×25; H-E stain) shows that the lesion consists predominantly of vascular sinusoids *(S)* surrounded by thin and thicker cellular septa (arrows). **(b)** Higher-magnification photomicrograph (original magnification, ×250; H-E stain) shows scant osteoid (arrows) produced by the pleomorphic tumor cells.

Characteristic radiographic appearances of telangiectatic OS include asymmetric expansion, geographic lysis of bone, and an aggressive growth pattern with cortical destruction and minimal peripheral sclerosis (Fig 19) (1,23,24). Pathologic fracture is also frequent (43%–61% of cases) (1,23). Common CT features of telangiectatic OS include a soft-tissue mass with attenuation lower

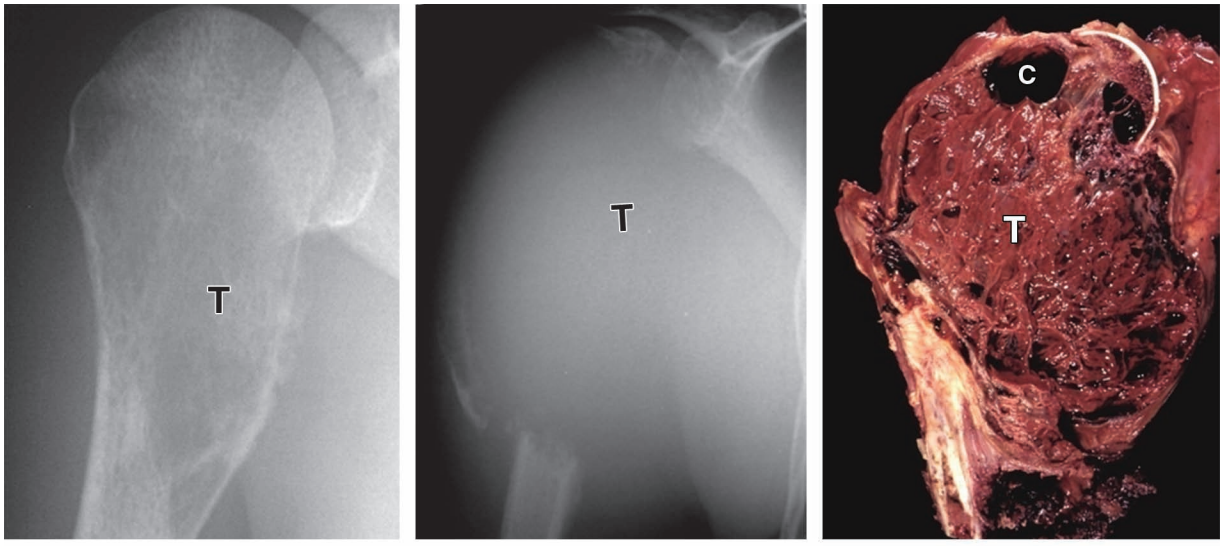

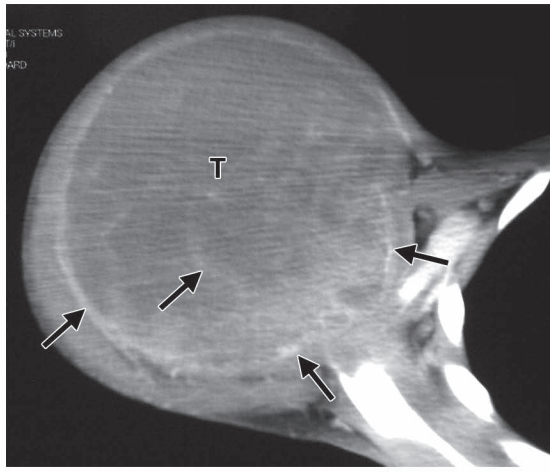

Figure 19. Telangiectatic OS in a 30-year-old man. **(a)** Initial radiograph of the proximal humerus reveals a lytic lesion *(T)*. **(b)** Radiograph obtained at 3-month follow-up shows that the lesion *(T)* has rapidly grown and is markedly expansile. **(c)** Photograph of a coronal section of the gross specimen shows the extremely hemorrhagic tumor *(T)* containing cystic areas *(C)*. **(d)** Axial contrast material–enhanced CT image shows multiple sites of peripheral and septal enhancement (arrows) within the tumor *(T)*. (Fig 19a–19d reprinted, with permission, from reference 1.)

than that of muscle, osteoid matrix mineralization, fluid levels, and thick peripheral and nodular septal enhancement (Fig 19). The enhancing thick rim and septa correspond to viable high-grade sarcomatous tissue in hemorrhagic or necrotic spaces; osteoid matrix mineralization occurs only in the viable neoplastic tissue in these areas (24). Osteoid matrix mineralization is often subtle on radiographs and of limited extent because viable tumor cells make up only a small amount of the lesion compared with the volume of cystic spaces. This subtle osteoid is more easily detected at CT (85%) than at radiography (58%) (24). At MR imaging, hemorrhage (high signal intensity on T1-weighted images and variable signal intensity on T2-weighted images) and fluid levels are frequently identified (96% and 74% of cases, respectively) (Fig 20) (24).

Radiologic differential diagnoses include ABC, giant cell tumor (GCT) of bone, metastases, and chondroblastic conventional OS. Distinguishing ABC from telangiectatic OS can be challenging because of histologic and radiologic similarities. Similar to telangiectatic OS, ABC can be hypervascular and demonstrates progressive osteolytic bone expansion and hemorrhage with fluid levels at CT or MR imaging (Fig 21). However, ABC typically shows only an enhancing thin peripheral rim and septa without nodularity or osteoid matrix mineralization. Furthermore, the pattern of growth in ABC is frequently less aggressive, with expansile remodeling and a well-defined

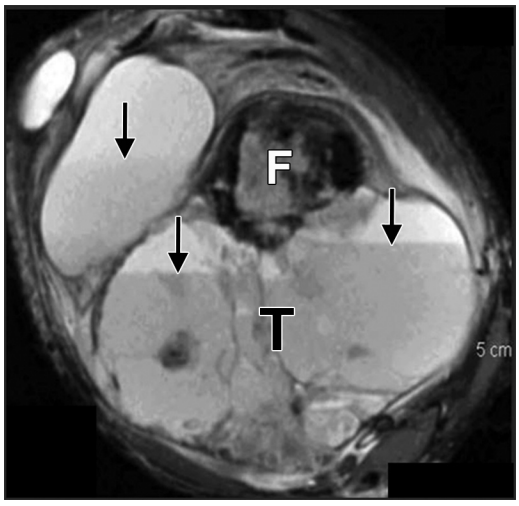

Figure 20. Telangiectatic OS in the thigh of a teenage patient. Axial proton-density–weighted MR image of the distal femur *(F)* shows an expansile and mostly cystic extraosseous mass *(T)* with multiple fluid levels (arrows).

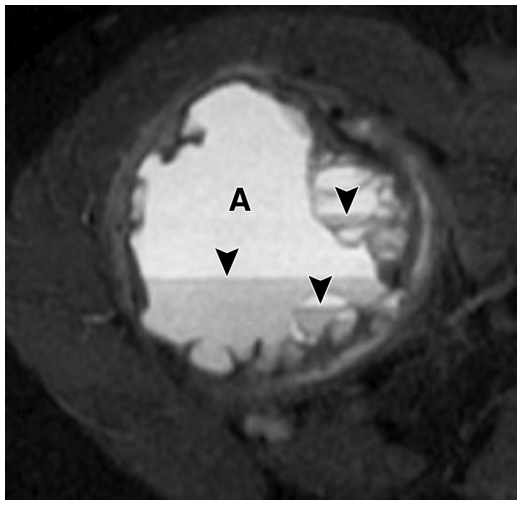

Figure 21. ABC in a 10-year-old boy. Axial short inversion time inversion-recovery MR image of the proximal humerus shows multiple fluid levels (arrowheads) within a lesion *(A)* without a soft-tissue mass.

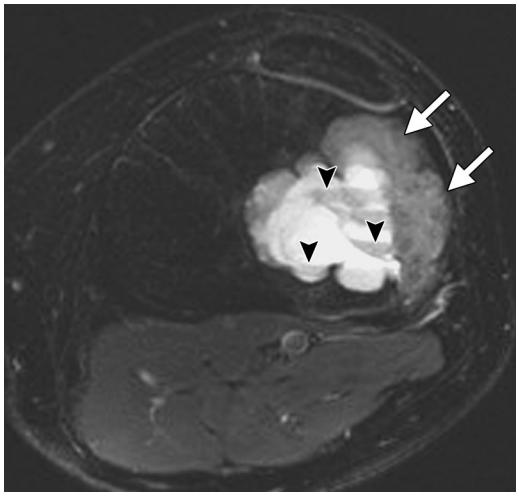

Figure 22. GCT in a 25-year-old woman. Axial T2-weighted fat-suppressed MR image shows a lesion of the tibia. The lesion has a cystic component that contains multiple fluid levels (arrowheads) and a soft-tissue component that demonstrates low signal intensity (arrows).

encapsulated margin, in contrast to the cortical destruction and infiltrative margins seen in telangiectatic OS. Therefore, the presence of nodular septal thickening, osteoid matrix mineralization in a soft-tissue mass, and an aggressive growth pattern can aid in distinguishing telangiectatic OS from ABC.

Teaching Point

GCT is another hemorrhagic tumor with an expansile lytic radiographic appearance that can be confused with telangiectatic OS (Fig 22). GCT is usually located at the end of the bone, close to the subchondral bone, and is a solid mass with intermediate signal intensity similar to that of muscle on T1-weighted MR images and low to intermediate signal intensity on T2-weighted MR images (27); these features contrast with the metadiaphyseal location and entirely cystic appearance of telangiectatic OS. Secondary ABC is a well-recognized entity, occurring in 14% of cases of GCT (27). GCT is the most common primary lesion associated with secondary ABC (28) and typically manifests with one quadrant as a solid lesion (Fig 22), in contrast to the nearly completely cystic appearance of telangiectatic OS.

Lytic metastases may mimic telangiectatic OS at radiography but can readily be distinguished at cross-sectional imaging, which demonstrates the presence of soft tissue without fluid levels. Renal metastases are known to exhibit flow voids at MR

imaging, a helpful feature in diagnosis. Conventional OS can be purely lytic when it is predominantly fibroblastic, but at CT or MR imaging, it is heterogeneously solid and lacks fluid levels.

Small Cell Osteosarcoma

Small cell OS constitutes approximately 1% of all OS cases (2) and most often affects patients in the 2nd and 3rd decades of life. These lesions are commonly located in the metaphyseal region of long bones (Fig 23) and most frequently involve the femur, but a minority (14%) are purely diaphyseal (29,30). With a 5-year survival rate of approximately 42%–50%, patients with small cell OS have a prognosis slightly less favorable than those with conventional OS (53%–61%) and Ewing sarcoma (51%) (2,3).

At histologic analysis, small cell OS may be mistaken for Ewing sarcoma or primitive neuroectodermal tumor because its cells are small and have round, hyperchromatic nuclei with little of the nuclear pleomorphism that is characteristic of conventional OS (Fig 24) (31). However, production of osteoid matrix by tumor cells must always be identified to make the diagnosis of OS. Furthermore, exclusion of the *EWS-ETS* chromosome 22 rearrangement associated with the Ewing sarcoma family of tumors is crucial, because small cell OS and Ewing sarcoma can appear very similar to each other at histologic analysis (1).

The radiographic features of small cell OS include permeative lytic bone destruction (in all cases), a soft-tissue mass, and periosteal reaction (>50% of cases) (Fig 25) (4,29). In small cell OS, calcification in the intramedullary cavity or an associated extraosseous soft-tissue mass at radiography or CT is frequent (>50% of cases) (29) and is a helpful diagnostic clue that the lesion is an osteoid matrix producing small cell OS (Fig 25).

Diagnostic considerations include Ewing sarcoma, lymphoma, and conventional OS. In particular, Ewing sarcoma is difficult to differentiate from small cell OS because of its histologic and radiologic resemblance to the latter. Although calcifications can be caused by the dystrophic process in necrotic tumor or extension of periosteal reaction (32), calcifications rarely occur in Ewing sarcoma (29,32) and are therefore useful for distinguishing between small cell OS and Ewing sarcoma. Other features that allow differentiation of Ewing sarcoma from small cell OS include cortical thickening (21% of cases) and cortical saucerization (6% of cases) (33) (Fig 26). Cortical saucerization is caused by local periosteal

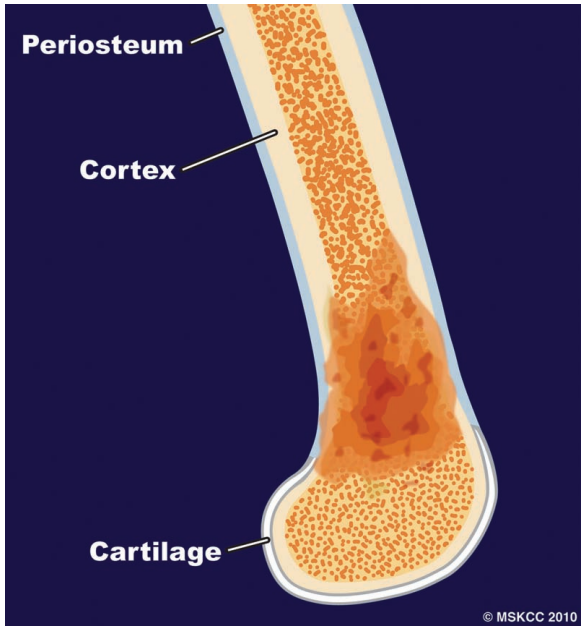

Figure 23. Drawing of small cell OS shows that the tumor most commonly arises from the metaphysis of a long bone and is permeative and lytic, involving the medullary canal.

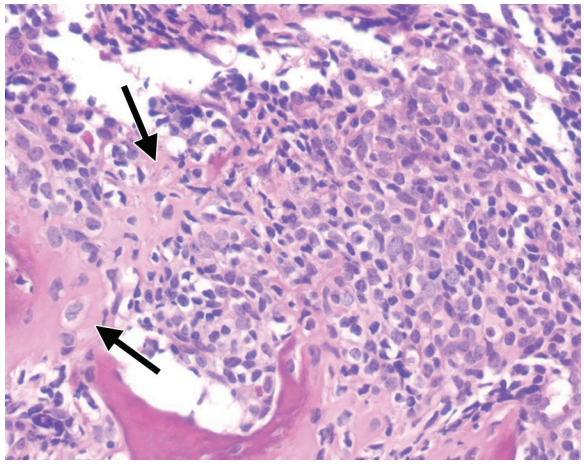

Figure 24. Histologic features of small cell OS. Photomicrograph (original magnification, ×400; H-E stain) shows that the tumor is composed of uniform, small, round blue cells resembling those of Ewing sarcoma; however, there is early bone or osteoid formation (arrows).

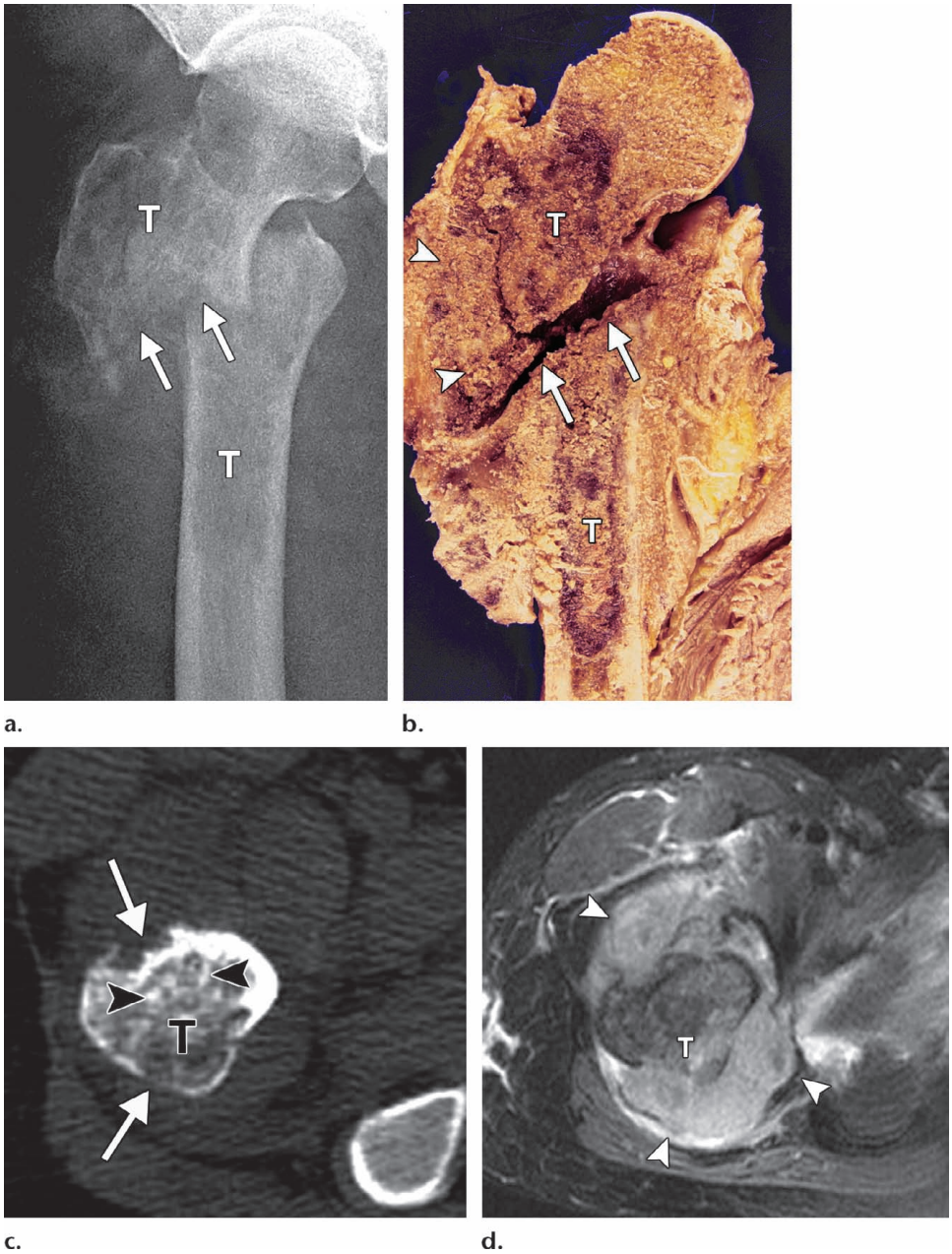

Figure 25. Small cell OS in a 26-year-old man. **(a)** Radiograph of the proximal femur shows a poorly defined lytic lesion *(T)* with a displaced pathologic fracture (arrows). **(b)** Photograph of a coronal section of the gross specimen shows the intramedullary lesion *(T)* and an extraosseous soft-tissue mass (arrowheads) associated with pathologic fractures (arrows). **(c)** Axial nonenhanced CT image shows the permeative lytic tumor *(T)* with calcifications (arrowheads) and cortical destruction (arrows). Because the soft-tissue mass is isoattenuating relative to muscle, it is difficult to detect without intravenous contrast material. **(d)** Axial T2-weighted fat-suppressed MR image shows the circumferential extraosseous soft-tissue mass (arrowheads) and intramedullary tumor *(T)*.

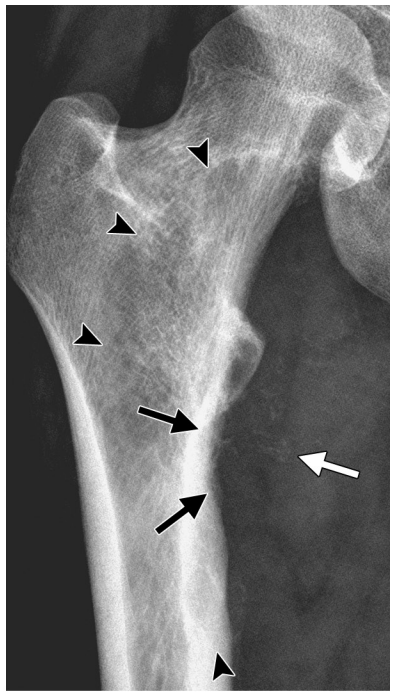

a.

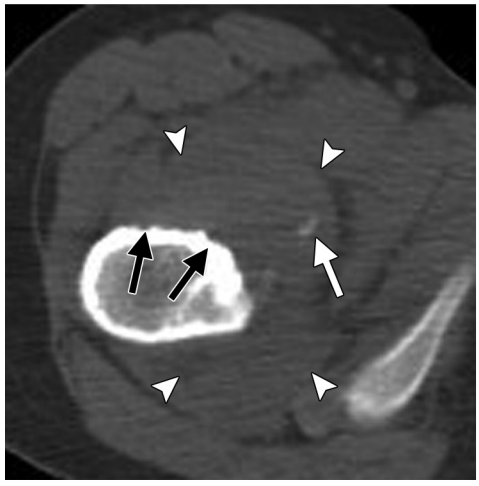

b.

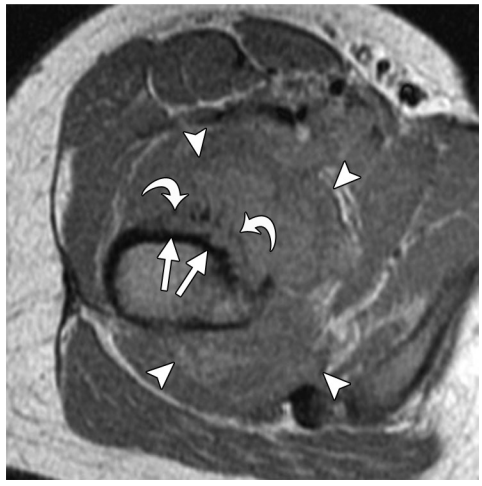

c.

Figure 26. Ewing sarcoma in a 14-year-old girl. **(a)** Radiograph of the proximal femur shows a permeative lytic lesion (arrowheads) and cortical saucerization (black arrows). The inferior border of the lesion is poorly defined. Subtle calcifications (white arrow) are seen in the soft-tissue mass. **(b, c)** Axial nonenhanced CT image **(b)** and axial T1-weighted MR image **(c)** obtained at the level of the lesser trochanter show the extraosseous soft-tissue mass (arrowheads). The cortical saucerization (black arrows in **b**, straight arrows in **c**) and soft-tissue calcification (white arrow in **b**) are also seen. The periosteum (curved arrows in **c**) is elevated by the tumor, which erodes into the underlying cortex (black arrows in **b**, straight arrows in **c**).

destruction by tumor and surrounding periosteal reaction, whereas pressure erosion is bone remodeling by a mass outside the bone (33).

Lymphoma of bone is a permeative lytic lesion commonly associated with extraosseous masses (48% of cases) (34); like Ewing sarcoma, lymphoma is able to spread outside of bone without osseous destruction (Fig 27). However, calcifications are uncommon in lymphoma before therapy, although sequestrum is occasionally found at pretherapy cross-sectional imaging (16% of cases) (34). In general, histopathologic appearances and immunohistochemical findings readily allow distinction between small cell OS and its differential diagnostic entities.

Low-Grade Central Osteosarcoma

Low-grade central OS is an uncommon subtype (<1% of OS cases) (35). The mean age at presentation is in the 3rd or 4th decade of life, and it commonly occurs within the medullary canal of the distal femur and proximal tibia (Fig 28) (36).

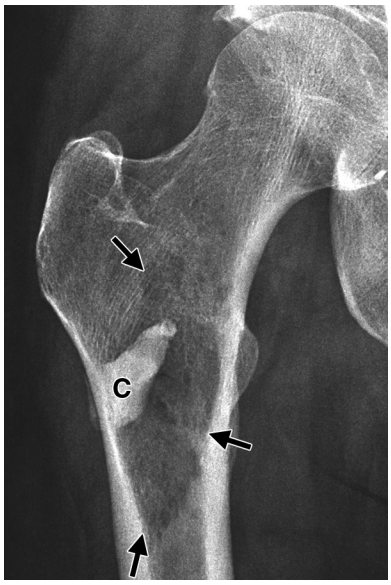

Figure 27. Large B-cell lymphoma in a 48-year-old woman. Radiograph shows a permeative lytic lesion (arrows) in the intertrochanteric femur. Periosteal reaction is scant due to tumor growth through cortical vessels without bone destruction. *C* = cement packing from biopsy.

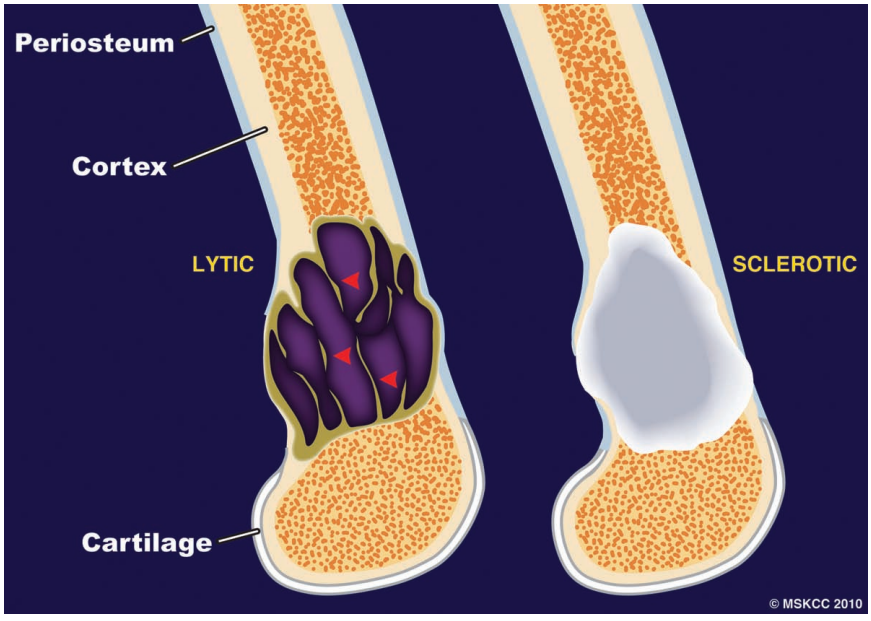

Figure 28. Drawings of low-grade central OS show that the tumor most commonly arises from the medullary canal of the metaphysis of the femur or tibia and has variable patterns of bone involvement. Expansile and lytic destruction with septal trabeculation (arrowheads) is the most common pattern (left); homogeneous sclerosis is also seen (right). Aggressive features such as cortical or medullary bone destruction and an extraosseous mass suggest the malignant nature, even if it is focal and subtle.

The prognosis for patients with low-grade central OS is substantially better than that for patients with conventional OS, with a 5-year survival rate of 90% (37). However, if treated with inadequate surgical margins, this tumor has the potential for dedifferentiation, local recurrence, and metastatic spread (38).

At histologic analysis, low-grade central OS is composed of a microtrabecular osseous matrix in a bland fibrous stroma with a variable amount of bone production. This histologic pattern is similar to that seen in fibrous dysplasia and fibrous

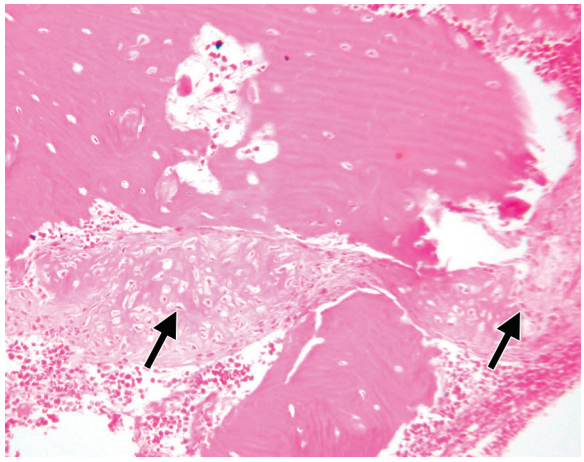

Figure 29. Histologic features of low-grade central OS. Photomicrograph (original magnification, ×160; H-E stain) shows the lamellar compacta of the cortex infiltrated by immature osteoid (arrows).

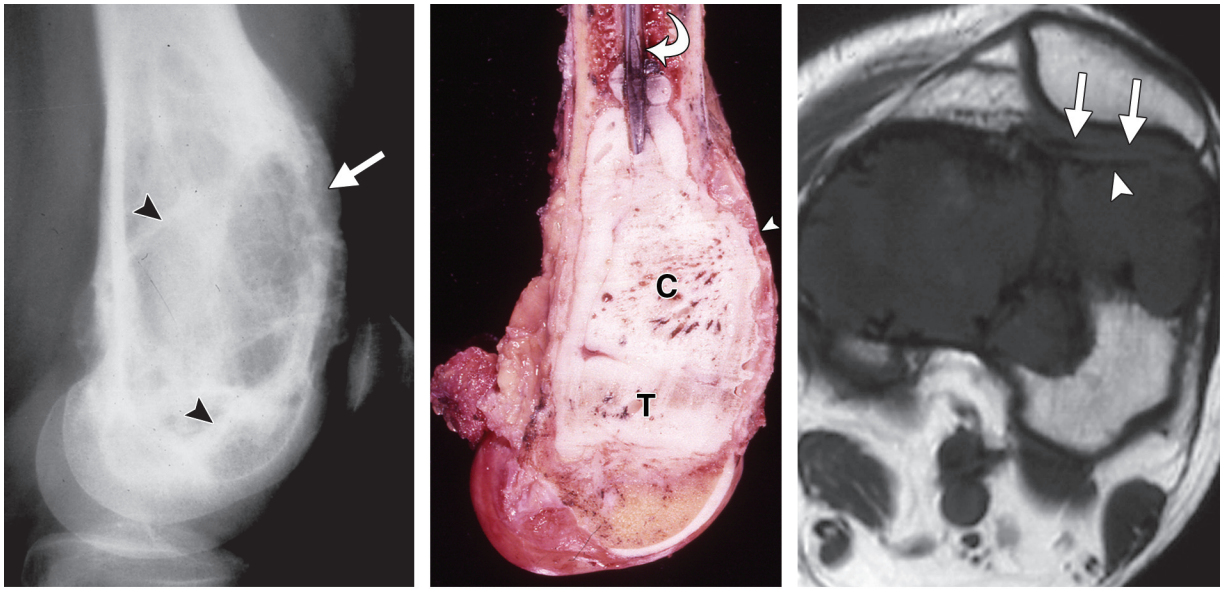

a. **b.** **c.**

Figure 30. Low-grade central OS in a 51-year-old man. **(a)** Radiograph of the knee shows an expansile and lytic lesion in the distal femoral metaphysis. The lesion contains multiple irregular thick trabeculae (arrowheads) and causes subtle anterior cortical destruction (arrow). **(b)** Photograph of a sagittal section of the gross specimen shows the intramedullary lesion *(T)*, which causes bone expansion and irregular thinning of the anterior cortex with focal destruction (arrowhead). Cement *(C)* is seen in the center of the lesion, and a fixation pin (arrow) is partially visualized. The patient initially underwent curettage of the lesion, cementing, and fixation with a pin because of a preoperative diagnosis of a presumed benign fibrous tumor. **(c)** Axial T1-weighted MR image shows subtle extraosseous extension of the tumor (arrows), an aggressive feature that allows differentiation from benign fibrous lesions. Arrowhead = cortex.

osseous lesions, but it most often resembles the histologic features of low-grade parosteal OS (1). Therefore, low-grade central OS is considered the intramedullary equivalent of low-grade parosteal OS (36), and both entities are usually treated with surgical resection alone. The permeative extension of tumor cells between mature bone trabeculae or into cortical bone is the key feature that allows differentiation of low-grade central OS from benign fibrous lesions (Fig 29).

Radiographic features of low-grade central OS are variable (36,38). The most common radiographic appearance is expansile lytic bone destruction with coarsely thick or thin incomplete trabeculation (61% of cases) (Fig 30) (36). A dense sclerotic pattern is less common (<30% of cases) (36). Cortical disruption and soft-tissue extension are common at CT and MR imaging (Fig 30); either of them was seen in all 31 cases with available CT and MR images in a study of 70 patients (36). Variable rates of periosteal reaction (22%–50%) at radiography are also reported (36,38).

Differential radiologic diagnoses include benign fibro-osseous lesions such as fibrous dysplasia, nonossifying fibroma, and desmoplastic fibroma. The presence of aggressive imaging features such as cortical destruction, soft-tissue extension, and periosteal reaction is a helpful clue for differentiation of low-grade central OS from benign fibro-osseous lesions, as these features are unusual in benign lesions.

Teaching Point

Conclusions

The classification of nonconventional subtypes of primary OS is based not only on histologic features but also on gross morphologic features, which are reflected at imaging. Each subtype exhibits distinct radiologic features that may be mimicked by various benign and malignant entities. For accurate diagnosis, it is important to be aware of radiographic and cross-sectional imaging features that allow differentiation of each nonconventional subtype of OS from its mimics.

Acknowledgments.—The authors thank Ada Muellner, MS, for editing and Terry Helms for the drawings and illustrations.

References

1. Klein MJ, Siegal GP. Osteosarcoma: anatomic and histologic variants. Am J Clin Pathol 2006;125(4):555–581.
2. Damron TA, Ward WG, Stewart A. Osteosarcoma, chondrosarcoma, and Ewing's sarcoma: National Cancer Data Base report. Clin Orthop Relat Res 2007;459:40–47.
3. Mirabello L, Troisi RJ, Savage SA. Osteosarcoma incidence and survival rates from 1973 to 2004: data from the Surveillance, Epidemiology, and End Results Program. Cancer 2009;115(7):1531–1543.
4. Murphey MD, Robbin MR, McRae GA, Flemming DJ, Temple HT, Kransdorf MJ. The many faces of osteosarcoma. RadioGraphics 1997;17(5):1205–1231.
5. Fletcher CDM, Unni KK, Mertens F, eds. Pathology and genetics of tumours of soft tissue and bone. In: World Health Organization classification of tumours. Lyon, France: IARC Press, 2002.
6. Antonescu CR, Huvos AG. Low-grade osteogenic sarcoma arising in medullary and surface osseous locations. Am J Clin Pathol 2000;114(suppl):S90–S103.
7. Jelinek JS, Murphey MD, Kransdorf MJ, Shmookler BM, Malawer MM, Hur RC. Parosteal osteosarcoma: value of MR imaging and CT in the prediction of histologic grade. Radiology 1996;201(3):837–842.
8. Campanacci M, Picci P, Gherlinzoni F, Guerra A, Bertoni F, Neff JR. Parosteal osteosarcoma. J Bone Joint Surg Br 1984;66(3):313–321.
9. Rose PS, Dickey ID, Wenger DE, Unni KK, Sim FH. Periosteal osteosarcoma: long-term outcome and risk of late recurrence. Clin Orthop Relat Res 2006;453:314–317.
10. Okada K, Frassica FJ, Sim FH, Beabout JW, Bond JR, Unni KK. Parosteal osteosarcoma: a clinicopathological study. J Bone Joint Surg Am 1994;76(3):366–378.
11. Bertoni F, Bacchini P, Staals EL, Davidovitz P. Dedifferentiated parosteal osteosarcoma: the experience of the Rizzoli Institute. Cancer 2005;103(11):2373–2382.
12. Sheth DS, Yasko AW, Raymond AK, et al. Conventional and dedifferentiated parosteal osteosarcoma: diagnosis, treatment, and outcome. Cancer 1996;78(10):2136–2145.
13. Murphey MD, Choi JJ, Kransdorf MJ, Flemming DJ, Gannon FH. Imaging of osteochondroma: variants and complications with radiologic-pathologic correlation. RadioGraphics 2000;20(5):1407–1434.
14. Lin J, Yao L, Mirra JM, Bahk WJ. Osteochondroma-like parosteal osteosarcoma: a report of six cases of a new entity. AJR Am J Roentgenol 1998;170(6):1571–1577.
15. Kransdorf MJ, Meis JM, Jelinek JS. Myositis ossificans: MR appearance with radiologic-pathologic correlation. AJR Am J Roentgenol 1991;157(6):1243–1248.
16. Robinson P, White LM, Sundaram M, et al. Periosteal chondroid tumors: radiologic evaluation with pathologic correlation. AJR Am J Roentgenol 2001;177(5):1183–1188.
17. Vanel D, De Paolis M, Monti C, Mercuri M, Picci P. Radiological features of 24 periosteal chondrosarcomas. Skeletal Radiol 2001;30(4):208–212.
18. Murphey MD, Jelinek JS, Temple HT, Flemming DJ, Gannon FH. Imaging of periosteal osteosarcoma: radiologic-pathologic comparison. Radiology 2004;233(1):129–138.
19. Revell MP, Deshmukh N, Grimer RJ, Carter SR, Tillman RM. Periosteal osteosarcoma: a review of 17 cases with mean follow-up of 52 months. Sarcoma 2002;6(4):123–130.

20. Staals EL, Bacchini P, Bertoni F. High-grade surface osteosarcoma: a review of 25 cases from the Rizzoli Institute. Cancer 2008;112(7):1592–1599.
21. Okada K, Unni KK, Swee RG, Sim FH. High grade surface osteosarcoma: a clinicopathologic study of 46 cases. Cancer 1999;85(5):1044–1054.
22. Vanel D, Picci P, De Paolis M, Mercuri M. Radiological study of 12 high-grade surface osteosarcomas. Skeletal Radiol 2001;30(12):667–671.
23. Weiss A, Khoury JD, Hoffer FA, et al. Telangiectatic osteosarcoma: the St. Jude Children's Research Hospital's experience. Cancer 2007;109(8):1627–1637.
24. Murphey MD, wan Jaovisidha S, Temple HT, Gannon FH, Jelinek JS, Malawer MM. Telangiectatic osteosarcoma: radiologic-pathologic comparison. Radiology 2003;229(2):545–553.
25. Huvos AG, Rosen G, Bretsky SS, Butler A. Telangiectatic osteogenic sarcoma: a clinicopathologic study of 124 patients. Cancer 1982;49(8):1679–1689.
26. Rezeanu L, Baker AC, Siegal GP, Klein MJ. Is better chemotherapy response in telangiectatic osteosarcoma due to increased tumor vascularization or higher proliferation index? A comparative immunohistochemical study of 20 cases. Presented at the annual meeting of the United States and Canadian Academy of Pathology, San Diego, Calif, March 24–30, 2007.
27. Murphey MD, Nomikos GC, Flemming DJ, Gannon FH, Temple HT, Kransdorf MJ. Imaging of giant cell tumor and giant cell reparative granuloma of bone: radiologic-pathologic correlation. RadioGraphics 2001;21(5):1283–1309.
28. Kransdorf MJ, Sweet DE. Aneurysmal bone cyst: concept, controversy, clinical presentation, and imaging. AJR Am J Roentgenol 1995;164(3):573–580.
29. Nakajima H, Sim FH, Bond JR, Unni KK. Small cell osteosarcoma of bone: review of 72 cases. Cancer 1997;79(11):2095–2106.
30. Ayala AG, Ro JY, Papadopoulos NK, Raymond AK, Edeiken J. Small cell osteosarcoma. Cancer Treat Res 1993;62:139–149.
31. Sim FH, Unni KK, Beabout JW, Dahlin DC. Osteosarcoma with small cells simulating Ewing's tumor. J Bone Joint Surg Am 1979;61(2):207–215.
32. Edeiken J, Raymond AK, Ayala AG, Benjamin RS, Murray JA, Carrasco HC. Small-cell osteosarcoma. Skeletal Radiol 1987;16(8):621–628.
33. Reinus WR, Gilula LA. Radiology of Ewing's sarcoma: Intergroup Ewing's Sarcoma study (IESS). RadioGraphics 1984;4(6):929–944.
34. Mulligan ME, McRae GA, Murphey MD. Imaging features of primary lymphoma of bone. AJR Am J Roentgenol 1999;173(6):1691–1697.
35. Unni KK, Dahlin DC, McLeod RA, Pritchard DJ. Intraosseous well-differentiated osteosarcoma. Cancer 1977;40(3):1337–1347.
36. Andresen KJ, Sundaram M, Unni KK, Sim FH. Imaging features of low-grade central osteosarcoma of the long bones and pelvis. Skeletal Radiol 2004;33(7):373–379.
37. Choong PF, Pritchard DJ, Rock MG, Sim FH, McLeod RA, Unni KK. Low grade central osteogenic sarcoma: a long-term followup of 20 patients. Clin Orthop Relat Res 1996;322(322):198–206.
38. Kurt AM, Unni KK, McLeod RA, Pritchard DJ. Low-grade intraosseous osteosarcoma. Cancer 1990;65(6):1418–1428.

RadioGraphics

Imaging Chatracteristics of Primary Osteosarcoma: Nonconventional Subtypes

Gail Yarmish, MD • Michael J. Klein, MD • Jonathan Landa, DO • Robert A. Lefkowitz, MD • Sinchun Hwang, MD

RadioGraphics 2010; 30:1653–1672 • **Published online** 10.1148/rg.306105524 • **Content Codes:** MK OI

Page 1656 (Figure on page 1657)
In contrast to osteochondroma, parosteal OS lacks corticomedullary continuity between the tumor and the underlying medullary canal (Fig 7).

Page 1659 (Figure on page 1655)
The ossification pattern of parosteal OS is the radiographic inverse of that seen in myositis ossificans, with the densest ossification in the center of the lesion and the least radiopaque bone at the periphery (Fig 3).

Page 1661 (Figure on page 1658)
Periosteal chondroid tumors are juxtacortical soft-tissue masses with well-defined borders, typically metaphyseal in location, and contain curvilinear calcifications along the periphery of the cartilage lobules (17) (Fig 10); in contrast, periosteal OS is a broad-based soft-tissue mass, commonly diaphyseal in location, and produces a cortical erosion and periosteal reaction perpendicular to the cortex (18).

Page 1665
Therefore, the presence of nodular septal thickening, osteoid matrix mineralization in a soft-tissue mass, and an aggressive growth pattern can aid in distinguishing telangiectatic OS from ABC.

Page 1671
The presence of aggressive imaging features such as cortical destruction, soft-tissue extension, and periosteal reaction is a helpful clue for differentiation of low-grade central OS from benign fibro-osseous lesions, as these features are unusual in benign lesions.